Publications of the Astronomical Society of the Pacific, 132:044201 (5pp), 2020 April https://doi.org/10.1088/1538-3873/ab77d8

An AGB Star with a Thick Circumstellar Shell

Jeremy Mould[1], Mark Durré[1], Syed Uddin[2], and Lifan Wang[3,4]
[1] Centre for Astrophysics & Supercomputing, Swinburne University, P.O. Box 218, Hawthorn, Vic 3122, Australia; jmould@swin.edu.au
[2] Carnegie Observatories, 813 Santa Barbara St, Pasadena, CA, USA
[3] Mitchell Institute for Fundamental Physics and Astronomy, Texas A&M University, College Station, TX 77843, USA
[4] Purple Mountain Observatory, Nanjing, 201008, Jiangsu, People's Republic of China
Received 2019 December 11; accepted 2020 February 19; published 2020 March 13

Abstract

The Asymptotic Giant Branch is the terminal phase of red giant evolution with timescales of millions of years and a total mass lost from the star that is a significant fraction of the initial mass. Investigation of one of these stars, WISEA J173046.10–344455.5, a kpc in the direction of the center of the Galaxy, reveals a cool oxygen rich star with a dust shell of blackbody temperature 1305 K.

Key words: stars: AGB and post-AGB – stars: mass-loss – stars: variables: general

Online material: color figures

1. Introduction

It will soon be 50 years since astrophysicists first evolved stellar models of low and intermediate mass stars beyond core helium burning to the double shell source phase. They encountered a number of phenomena not seen in simpler structures: thermal pulses and convective troughs which mixed burning products to the surface, terminal mass loss leading to the exposure of hot cores (and planetary nebulae), a powerful observational constraint in the form of the initial final mass relation, an instability region in the cool HR diagram and a rapid luminosity evolution (1 mag per million years).

Unsurprisingly, infrared observations have proved illuminating of this phase of evolution. The Magellanic Clouds have proved a valuable laboratory (Frogel et al. 1990; Cioni 2004; Meixner et al. 2008). Much complexity remains to be explored, and *Gaia*'s Galactic distances can be expected to provide a solar metallicity contrast with what has been discovered there.

Among the problems still challenging AGB evolution are hydrodynamic treatment of stellar and circumstellar structure, single star loss winds and binary mass transfer. AGB stars are the stellar site for the main s-process (slow neutron capture process), with ^{13}C being the major neutron source via $^{13}C(\alpha,n)^{16}O$ (Gallino et al. 1998; Karakas 2018), with challenges to develop a quantitative treatment. We can expect progress with the advance of more powerful observations at high spatial and spectral resolution.

The optical transient AT2019gac was discovered on 2019 May 27 by the MASTER Global Robotic Net (MASTER OT J173045.95-344454.7),[5] with a discovery magnitude of 16.5. Rather than discard it as a non-supernova on the basis of the spectrum, we pursued it as a long period variable (LPV) star. This was spatially identified with WISEA J173046.10–344455.5 (2MASS J17304612–3444551), henceforth J173046. The 2MASS and *Wide-field Infrared Survey Explorer* (*WISE*) color images are shown in Figure 1, illustrating the redness of the object. Infrared spectroscopy and photometry show that it is a luminous asymptotic giant branch (AGB) star with a large, thick, and cool circumstellar shell, located in a region a kpc from the Sun toward the Galactic Center, that has been actively forming stars in the last 0.1–1 Gyr.

[5] https://wis-tns.weizmann.ac.il/object/2019gac

2. Optical Spectrum and Distance

J173046 has a very red color ($i - z = 3.84$ from SkyMapper data; Wolf et al. 2018). SkyMapper z images also show a decline in brightness of ∼0.5 mag over the period 2014 August 1 to 2018 March 14. The optical spectrum was obtained on 2019 June 13 with the WiFeS spectrograph (Dopita et al. 2007) on the ANU 2.3 m telescope at Siding Spring Observatory. A standard star was observed (Feige 110), the data were reduced using PyWiFeS software (Childress et al. 2014), and the spectrum (longward of 750 nm) is shown in Figure 2. Shortward of this, the spectrum is non-existent at the flux limit.

J173046 has also been observed by ESA's *Gaia* satellite (The Gaia Collaboration et al. 2016). Its parallax in DR2 is 0.921 ± 0.258 mas $= 1086(+422, -238)$ pc. (Bailer-Jones et al. 2018; The Gaia Collaboration et al. 2018) We neglect the DR2 parallax offset of –0.08 mas (Stassun & Torres 2018). The source catalog gives passband magnitudes of $m_G = 16.07 \pm 1.1$ and $m_{RP} = 14.1 \pm 1.05$, with the variability derived from the mean error in the fluxes. J173046 is not flagged as a variable in *Gaia* DR2; however, the are 135 g band

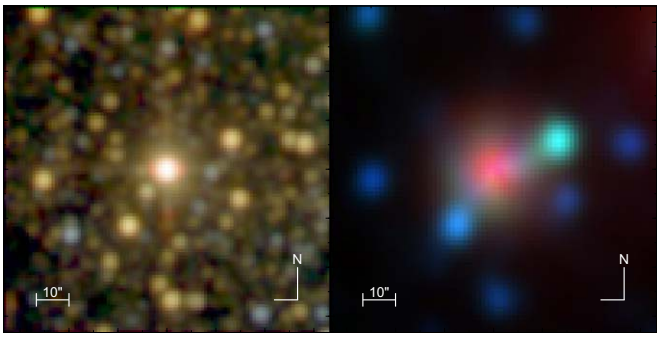

Figure 1. Color images of WISEA J173046.10–344455.5. Left: 2MASS $J/H/K_s$ (spatial resolution 1″/pixel—logarithmic scaling). Right: *WISE* $W1/W2/W3$ (spatial resolution 1.″375/pixel—linear scaling). Colors for each filter are blue/green/red correspondingly. The length scales and orientations are shown. The object is significantly redder than field stars.
(A color version of this figure is available in the online journal.)

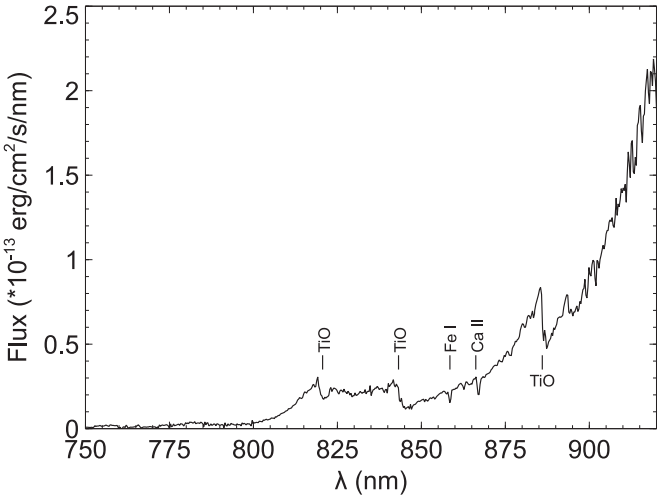

Figure 2. WiFeS spectrum of AT2019gac. The spectrum is a late M star, showing TiO bandheads and atomic absorption lines.

magnitude measurements yielding a 0.066 mag standard error on the mean. If it is a LPV, more observations are required to find a period.

J173046 is located in a region with a number of young star clusters: Collinder 133, ESO 392-13 and Ruprecht 126 (Kharchenko et al. 2013). Their distances from the Sun range from 0.8 to 2.3 kpc, their reddening from $E(B-V) = 0.11$–0.82 mag, and their ages from (0.9–8) $\times$ 10^8 yr.

3. IR Spectroscopy and Photometry

3.1. Spectroscopy

The steep rise in Figure 2 demands an infrared spectrum. This was observed with the SofI (Son of ISAAC) near-infrared (NIR) spectrometer (Moorwood et al. 1998) at the Nasmyth A focus of the ESO 3.5 m New Technology Telescope (NTT) at the European Southern Observatory (ESO) in La Silla (Chile), as a commensal observation in the program 0103.B-0504(B) (observation date 2019 August 25). Both the GBF and GRF grisms were used with a 1″ slit width, for a spectral range of 918–2518 nm and a spectral resolution $R \sim 600$. The A0 star HIP 79473 was also observed as a telluric standard and flux calibrator. The data were reduced in the standard manner, with flat-fielding, extraction of the spectrum from the A–B pair observations, wavelength calibration, and combination of all frames for each object. Telluric correction and flux calibration were performed using an A0V stellar spectral template (from the ESO stellar library of Pickles 1998). The GBF and GRF spectra were combined, showing excellent flux calibration at the boundary wavelength (1600 nm), as seen in Figure 3. The spectrum was re-dispersed to the range 940–2410 nm, with 0.5 nm steps.

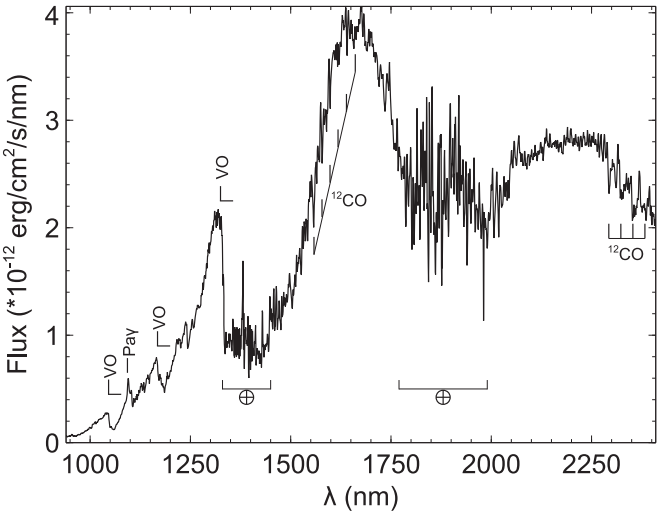

Figure 3. NIR Spectrum of AT2019gac. Note the noisy regions between the atmospheric windows, designated with ⊕ symbol (1330–1450 nm and 1770–1990 nm). Spectral features include the VO bandheads in the J band, plus CO in H and K bands. Paγ is identified in emission.

3.2. Photometry

J173046 has also been observed by NASA's *WISE* satellite (Wright et al. 2010; Cutri et al. 2013), and has 2MASS photometry (Skrutskie et al. 2006). Combining these with SkyMapper i and z data, we can plot the spectral energy distribution (SED), shown in Figure 4. A blackbody curve was fitted to the photometric points, yielding a best-fit temperature of 1305 K. The excess flux at the *WISE* $W3$ band can be attributed to silicate emissions at $\sim$10 μm.

Computing the integrated flux of the fitted blackbody, we obtain $F_{BB} = 1.47 \times 10^{-8}$ erg cm^{-2} s^{-1}. Equating the luminosity of a blackbody of radius R and temperature T with that

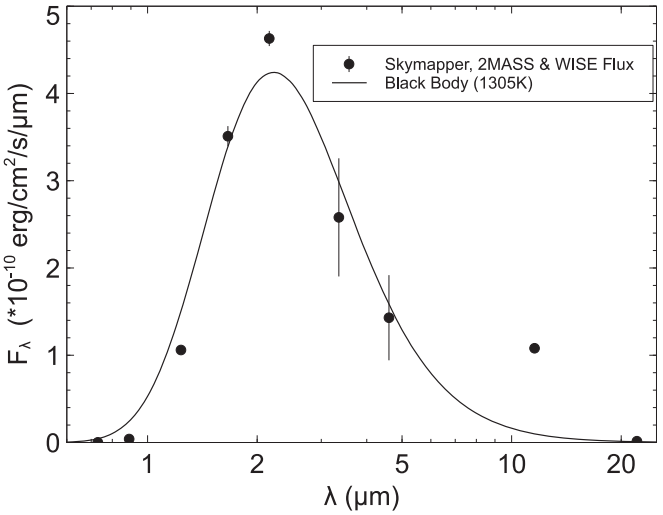

Figure 4. Spectral energy distribution from SkyMapper, 2MASS and *WISE* photometry. The flux units are 10^{-10} erg cm^{-2} s^{-1} μm^{-1}. The curve is a 1305 K blackbody.

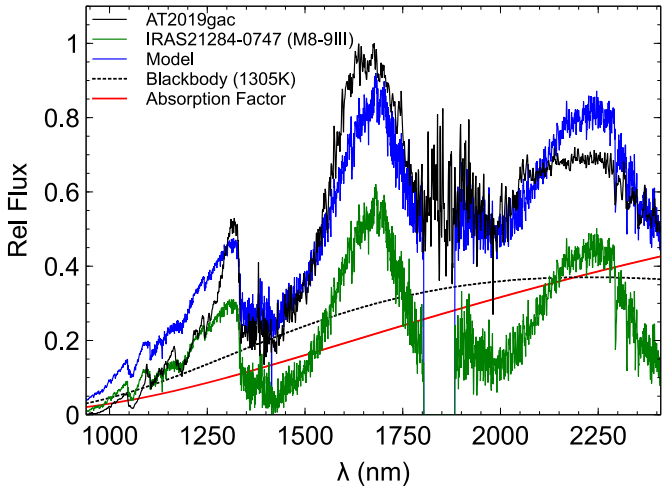

Figure 5. Model of a M8-9III stellar template fit to the IR spectrum of J173046 with an extinction $E(B-V) = 3.06$ (CCM law), plus a contribution from the circumstellar shell blackbody emission at 1305 K. The plot shows the observed spectrum (black), the template spectrum (green), the circumstellar shell absorption factor (red) and the blackbody contribution (dashed black), with the best fit model (blue). Fluxes are in arbitrary units and normalized.
(A color version of this figure is available in the online journal.)

derived from the observed flux at distance D (found above), we obtain the relationship:

$$R = \frac{D}{T^2}\sqrt{\frac{F_{BB}}{\sigma}} \quad (1)$$

where σ is the Stefan–Boltzmann constant.

From this we derive the radius of the dust shell $R = 455(+177, -101)\ \mathcal{R}^{\rm N}_{\odot}$ and luminosity $L = 540\ (+1340, -210)\ \mathcal{L}^{\rm N}_{\odot}$ (the uncertainties are from the range of *Gaia* distances). Given the solar bolometric magnitude of 4.75, this equates to $M_{\rm Bol} = -2.1(+0.6, -1.3)$.

4. Discussion

4.1. Spectral Type and the Dust Shell

The features of the spectrum (the broad bumps in the H and K spectral regions and the molecular features in the J band) are similar to a late-class M star, however with a different general slope. Inspecting the IRTF IR spectral library of cool stars (Rayner et al. 2009), we noticed a striking similarity to IRAS01037+1219 (WX Psc). This is classed as a variable of type M (OH/IR), i.e., a Mira at the very late stage of AGB evolution, with a highly dusty shell, extreme mass loss rate and OH maser emission. A search of the 1612 MHz OH blind survey of the galactic bulge region by Sevenster et al. (1997) [6] did not show a match.

Full treatment of the emission and absorption of the star and shell would require radiative transfer code like DUSTY (Ivezic et al. 1999), but this is beyond the scope of this paper. To determine the extinction (and thus the stellar magnitude), we can model the spectrum using a late M stellar template plus a standard dust extinction curve. We also include a contribution from the blackbody emission modeled by the SkyMapper, 2MASS and *WISE* data. Our model is thus:

$$F_\lambda = \alpha\, T_\lambda\, a_\lambda + \beta\, B_\lambda \quad (2)$$

where F_λ is the observed spectrum, T_λ is the template spectrum, B_λ is the blackbody contribution and a_λ is the wavelength-dependent absorption from the circumstellar shell. α and β are arbitrary scaling constants to be fitted.

We selected 8 stellar templates from the IRTF library with spectral type M7III to M9III. We modeled the extinction using both the Cardelli et al. (1989) (CCM) and the Calzetti et al. (2000) (CAL) curves, with the blackbody temperature fixed at 1305 K, as derived from the SED fit. The best fit was with the template IRAS 21284-0747 (HY Aqr), spectral type M8-9III. Both forms of the extinction curve gave similar results; the CCM extinction model gave sightly better fit, with an $E(B-V) = 3.06$. This translates to a V band extinction $A_V \approx 9.5$ mag (using the standard CCM factor $R_V = 3.1$). Allowing the blackbody temperature to vary in the fit produced almost no change.

The plot of this fit is shown in Figure 5. The fit broadly reproduces the features of the NIR spectrum; the broad peaks in the H and K and the molecular features in the J band combined with the steep decline in flux toward shorter wavelengths. The detailed flux levels are somewhat different, however this can be ascribed to (a) the differences in extinction between the dust shell and the CCM model and (b) differences in detail between

[6] http://cdsarc.u-strasbg.fr/viz-bin/cat/J/A+AS/122/79

the template and the stellar spectra. The circumstellar shell and the stellar emission contribute roughly equal amounts of flux over the NIR range.

At the effective wavelength of the 2MASS K_s filter (2159 nm), we fitted an extinction factor of 0.37 (=1.1 mag); with the range of *Gaia* distances the 2MASS magnitude ($K_s = 4.92 \pm 0.02$) translates to $M_K = -6.15 \pm 0.6$.

4.2. Comparison with Surveys

The most comprehensive study of cool star SEDs is the SAGE survey of the Magellanic Clouds (Meixner et al. 2006). Woods et al. (2011) assigns 13 classifications to point sources, and J173046 fits O-AGB better than a Young Stellar Object in this system; that is to say, it is an oxygen rich (M type) AGB star at the faint end of Woods's bolometric luminosity function. Without a firm period measurement, it is not possible to tell to which of four sequences of Wood (2000) of variable red giants J173046 belongs.

We can also compare this object to the study by Wood (2015) of variability of luminous red giants in the Large Magellanic Cloud (LMC). The Weisenheit reddening free magnitude of the object is

$$W_{JK} = K - 0.686\,(J - K). \quad (3)$$

This has a value of 2.33; at the distance of the LMC ($m - M = 18.45$), this translates to $W_{JK} = 10.8$, which is within the range for Wood's Figure 10 plot. Since there is an unknown contribution from the LMC's stars' circumstellar shells, we can only say that W_{JK} and K are plausible for AGB LPVs.

4.3. Mass Loss

Although we tend to associate thick dust shells with the terminal maximum luminosity phase of AGB evolution, it is quite possible from the point of view solely of the mass budget for a low luminosity AGB star to supply the requisite dust. A low or intermediate mass star may lose as much as $0.3\mathcal{M}_{\odot}^{\rm N}$ of gas at the time of the helium flash; after that the Reimers (1977) mass loss rate for a one solar mass star with the parameters we find here is of order $10^{-5}\,\mathcal{M}_{\odot}^{\rm N}\,{\rm yr}^{-1}$. Lebzelter & Wood (2005) have studied variable red giants in 47 Tuc with a luminosity $\log L/\mathcal{L}_{\odot}^{\rm N} = 3.15$, considerably below the tip of the red-giant branch (RGB) at $\log L/\mathcal{L}_{\odot}^{\rm N} = 3.35$. Models that have undergone mass loss reproduce observed period–luminosity relations and they show that mass loss of the order of $0.3\mathcal{M}_{\odot}^{\rm N}$ occurs along the RGB and AGB. They show that stars evolve up the RGB and first part of the AGB pulsating in low order overtone modes, then switch to fundamental mode at high luminosities.

Assuming a dust absorption coefficient of $0.4\,{\rm cm}^2\ {\rm gm}^{-1}$ (Chini et al. 1991) and a gas to dust ratio of 100, we can compute the gas mass required to give $A_V = 9.5$ mag; this is $M_{\rm Gas} = 4.9 \times 10^{-5}\mathcal{M}_{\odot}^{\rm N}$. Thus there is ample dust to provide an optically thick shell.

4.4. Possible Origin of the Transient

The transient was at least 1.5 mag visually brighter than its minimum (given the limiting magnitude of 17.9 for the MASTER network), but had faded over the 90 day period between discovery and our IR observation (our estimate from the IR spectrum is $K_S = 5.9$ mag, below that of the 2MASS catalog of 4.92 mag). The cause of the transient is not known; this could be intrinsic, e.g., the prototypical AGB LPV (Mira) has been shown to have X-ray flares on a 1–2 day timescale (Karovska et al. 2005) and the symbiotic Mira V407 Cyg produced a nova outburst (Munari et al. 2011). Extrinsically, the dust shell may not be uniform (e.g., Tatebe et al. 2008; Paladini et al. 2012), possibly caused by companions, stellar asymmetry, asymmetric dust emission or dust clumps.

5. Conclusion

The transient AT2019gac is identified with the very red object WISEA J173046.10–344455.5. The color is due to the late spectral type of the central red giant with some foreground reddening, but notably to a circumstellar shell of warm dust. This shell has an estimated temperature of 1305 K, a luminosity of 540 $\mathcal{L}_{\odot}^{\rm N}$ and a radius of 455 $\mathcal{R}_{\odot}^{\rm N}$. From the observed extinction, the gas mass is $4.9 \times 10^{-5}\mathcal{M}_{\odot}^{\rm N}$. On the basis of our observations, J173046 is a mass losing, LPV, AGB star, whose initial mass would have been comparable to the turnoff masses of the star clusters of its region in the Galaxy.

With a *WISE W4* mag of 1.34, J173046 would repay spectroscopy at 3–30 μm to investigate this shell in detail. We are only now beginning to get a good sample of Galactic LPV luminosities thanks to *Gaia* (e.g., Lebzelter et al. 2018).

We thank the reviewer for their constructive report, which much improved the paper. This paper is based on observations collected at the European Organisation for Astronomical Research in the Southern Hemisphere under ESO program 0103.B-0504(B). We thank Purple Mountain Observatory, Nanjing, PRC for its support of this program.

This work presents results from the European Space Agency (ESA) space mission *Gaia. Gaia* data are being processed by the *Gaia* Data Processing and Analysis Consortium (DPAC). Funding for the DPAC is provided by national institutions, in particular the institutions participating in the *Gaia* MultiLateral Agreement (MLA).

This publication makes use of data products from the *Wide-field Infrared Survey Explorer*, which is a joint project of the University of California, Los Angeles, and the Jet Propulsion Laboratory/California Institute of Technology, funded by the National Aeronautics and Space Administration (NASA) and from the Two Micron All Sky Survey, which is a joint project

of the University of Massachusetts and the Infrared Processing and Analysis Center/California Institute of Technology, funded by the NASA and the National Science Foundation.

The national facility capability for SkyMapper has been funded through ARC LIEF grant LE130100104 from the Australian Research Council, awarded to the University of Sydney, the Australian National University, Swinburne University of Technology, the University of Queensland, the University of Western Australia, the University of Melbourne, Curtin University of Technology, Monash University and the Australian Astronomical Observatory. SkyMapper is owned and operated by The Australian National University's Research School of Astronomy and Astrophysics.

Facilities: ATT:WiFeS, NTT:SofI, *Gaia*, NEOWISE, SkyMapper.

ORCID iDs

Jeremy Mould https://orcid.org/0000-0003-3820-1740
Mark Durré https://orcid.org/0000-0002-2126-3905
Syed Uddin https://orcid.org/0000-0002-9413-4186

References

Bailer-Jones, C. A. L., Rybizki, J., Fouesneau, M., et al. 2018, AJ, 156, 58
Calzetti, D., Armus, L., Bohlin, R. C., et al. 2000, ApJ, 533, 682
Cardelli, J. A., Clayton, G. C., & Mathis, J. S. 1989, ApJ, 345, 245
Childress, M. J., Vogt, F. P. A., Nielsen, J., & Sharp, R. G. 2014, Ap&SS, 349, 617
Chini, R., Kruegel, E., Kreysa, E., Shustov, B., & Tutukov, A. 1991, A&A, 252, 220
Cioni, M.-R. L. 2004, in ASP Conf. Ser. 310, IAU Coll. 193 Var. Stars Local Gr., ed. D. W. Kurtz & K. R. Pollard (San Francisco, CA: ASP), 149
Cutri, R. M., Wright, E. L., Conrow, T., et al. 2013, Explanatory Supplement to the AllWISE Data Release Products, http://wise2.ipac.caltech.edu/docs/release/allwise/expsup/index.html
Dopita, M., Hart, J., McGregor, P., et al. 2007, Ap&SS, 310, 255
Frogel, J. A., Mould, J., & Blanco, V. M. 1990, ApJ, 352, 96
Gallino, R., Arlandini, C., Busso, M., et al. 1998, ApJ, 497, 388
Ivezic, Z., Nenkova, M., & Elitzur, M. 1999, User Manual for DUSTY, https://github.com/ivezic/dusty/tree/master/dustyV2/Manual/manual.pdf
Karakas, A. I. 2018, Proc. IAU, 14, 79
Karovska, M., Schlegel, E., Hack, W., Raymond, J. C., & Wood, B. E. 2005, ApJL, 623, L137
Kharchenko, N. V., Piskunov, A. E., Schilbach, E., Röser, S., & Scholz, R.-D. 2013, A&A, 558, A53
Lebzelter, T., Mowlavi, N., Marigo, P., et al. 2019, Proc. IAU, 14, 73
Lebzelter, T., & Wood, P. R. 2005, A&A, 441, 1117
Meixner, M., Bernard, J. P., Blum, R. D., et al. 2008, Proc. IAU, 4, 3
Meixner, M., Gordon, K., Indebetouw, R., et al. 2006, AJ, 132, 2268
Moorwood, A., Cuby, J. G., & Lidman, C. 1998, Msngr, 91, 9
Munari, U., Joshi, V. H., Ashok, N. M., et al. 2011, MNRAS, 410, L52
Paladini, C., Sacuto, S., Klotz, D., et al. 2012, A&A, 544, L5
Pickles, A. J. 1998, PASP, 110, 863
Rayner, J. T., Cushing, M. C., & Vacca, W. D. 2009, ApJS, 185, 289
Reimers, D. 1977, A&A, 61, 217
Sevenster, M. N., Chapman, J. M., Habing, H. J., Killeen, N. E., & Lindqvist, M. 1997, A&AS, 122, 79
Skrutskie, M. F., Cutri, R. M., Stiening, R., et al. 2006, AJ, 131, 1163
The Gaia Collaboration, Prusti, T., de Bruijne, J. H. J., et al. 2016, A&A, 595, A1
The Gaia Collaboration, Spoto, F., Tanga, P., et al. 2018, A&A, 616, A13
Stassun, K. G., & Torres, G. 2018, ApJ, 862, 61
Tatebe, K., Chandler, A. A., Hale, D., & Townes, C. H. 2008, ApJ, 652, 666
Wolf, C., Onken, C. A., Luvaul, L. C., et al. 2018, PASA, 35, e010
Wood, P. 2015, MNRAS, 448, 3829
Wood, P. R. 2000, PASA, 17, 18
Woods, P. M., Oliveira, J. M., Kemper, F., et al. 2011, MNRAS, 411, 1597
Wright, E. L., Eisenhardt, P. R. M., Mainzer, A., et al. 2010, AJ, 140, 1868